Chimica Techno Acta
published by Ural Federal University
eISSN 2411-1414
chimicatechnoacta.ru

ARTICLE
2024, vol. 11(4), No. 202411409
DOI: 10.15826/chimtech.2024.11.4.09

Synthesis and evaluation of MMT/TiO_2 nanotube photocatalysts for enhanced degradation of organic dyes in wastewater

Bang Tam Thi Dao [ab *], Trung Do Nguyen [ab], Hon Nhien Le [ab], Chi-Nhan Ha-Thuc [ab **]

a: Faculty of Materials Science and Technology, University of Science, Viet Nam National University, Ho Chi Minh City, Ho Chi Minh City, Vietnam
b: Vietnam National University, Ho Chi Minh City, Vietnam
* Corresponding author: dtbtam@hcmus.edu.vn
** Corresponding author: htcnhan@hcmus.edu.vn

This paper belongs to a Regular Issue.

Abstract

This study aims to synthesize a nanocomposite photocatalyst from naturally sourced clay (montmorillonite, MMT) and titanium dioxide nanotubes (TNTs) to efficiently degrade organic dyes in wastewater under UVC light. The TNTs were synthesized through the hydrothermal method and were randomly attached to both the surface and interlayer spaces of the MMT sheets. Pristine MMT was found to exhibit good adsorption properties, while the TNTs demonstrated strong photocatalytic activity. The combination of these materials in the MMT/TNT nanocomposite resulted in a material that exhibited both adsorption and photocatalytic properties. The dye degradation efficiency of the MMT/TNT nanocomposite reached 95%, which is significantly higher than that of pristine MMT (50%) and TNTs alone (60%). This enhanced performance can be attributed to the synergistic effect between the adsorption capacity of MMT and the photocatalytic activity of TNTs. The study highlights the potential of using naturally sourced materials like MMT in the development of advanced photocatalysts for environmental remediation. The MMT/TNT nanocomposite offers a sustainable and efficient solution for the removal of organic pollutants from wastewater. These findings provide a pathway for further development of high-performance nanocomposites that combine the dual functional properties of adsorption and photocatalysis, contributing to more efficient wastewater treatment technologies.

Keywords

montmorillonite
TiO_2 nanotubes
nanocomposite
photocatalyst
degradation
organic dye
decolorization

Received: 29.03.24
Revised: 02.10.24
Accepted: 13.10.24
Available online: 23.10.24

Key findings

- MMT/TiO_2 nanotube nanocomposite achieved 95% dye degradation, outperforming pristine MMT (50%) and TiO_2 alone (60%).
- The MMT/TiO_2 nanocomposite combines strong adsorption from MMT with photocatalytic activity from TiO_2, enhancing overall performance.
- Utilizing natural MMT in the nanocomposite offers an efficient and sustainable method for removing organic pollutants from wastewater.

1. Introduction

Montmorillonite (MMT) is recognized as a very soft phyllosilicate mineral, belonging to the smectite group, and is classified as a 2:1 clay mineral. This structure consists of two tetrahedral sheets sandwiching a central octahedral sheet. MMT is the main component of bentonite, which forms through the weathering of volcanic ash. The water content in montmorillonite is variable and can significantly increase in volume when it absorbs moisture. Chemically, MMT is a hydrated sodium calcium aluminum magnesium

silicate hydroxide, $(Na,Ca)_{0.33}(Al, Mg)_2(Si_4O_{10})(OH)_2 \cdot nH_2O$. Potassium, iron, and other cations often substitute within its structure, with a specific ratio depending on the source. MMT is typically found in mixtures with chlorite, muscovite, illite, cookeite, and kaolinite [1–3]. Due to its layered structure and inherent porosity, MMT is widely used as a natural adsorbent or as a support material to enhance the specific surface area and adsorption capacity of catalysts [4, 5].

Numerous studies have explored the combination of MMT with metal oxide semiconductors [6], with prominent examples including TiO_2 [7], ZnO [8], and CuO [9]. These studies have shown considerable potential in enhancing photocatalytic efficiency through these combinations. However, challenges remain, such as the potential toxicity and limited biodegradability of certain materials. In this research, TNTs were synthesized via a hydrothermal method and then randomly immobilized onto MMT. The study assessed the ability of these composites to decolorize and degrade the organic dye Basic Blue 3 (BB3). Currently, research on TiO_2 nanotube structures immobilized on MMT is limited.

Previous studies have highlighted the effectiveness of TiO_2 nanotubes with various structures in photocatalysis. For instance, E. S. Ghalehsefid and colleagues successfully synthesized a TiO_2 nanotube/$ZnIn_2S_4$ nanoflower (TiO_2 NT/ZIS) composite heterojunction for the degradation of Rhodamine B. This photocatalyst, synthesized via a hydrothermal method, achieved a 90.2% degradation efficiency of RhB on the TiO_2NT/ZIS nanocomposite after 120 min [10]. However, $ZnIn_2S_4$ may contain toxic components or be challenging to biodegrade. Qingyao Wang and colleagues synthesized a TiO_2NTs/Sn_3O_4 photocatalyst through a hydrothermal method, depositing Sn_3O_4 onto TiO_2 nanotube arrays. Yet, this deposition process can lead to non-uniformity, affecting the photocatalytic performance [11]. Moreover, Sn_3O_4 might also contain harmful or non-biodegradable components, raising safety and environmental concerns. Yu-Long Xie and colleagues successfully deposited BiOI nanosheets onto three-dimensional porous TiO_2 nanotube arrays (NTs) using the successive ionic layer adsorption and reaction (SILAR) method, achieving a 93.5% degradation efficiency of RhB after 200 min under visible light [12]. However, ensuring the uniformity of BiOI nanosheets on TiO_2 NTs surfaces remains a challenge, as uneven deposition can negatively impact the material's photocatalytic performance.

While the materials and methods may differ, the studies have consistently highlighted the effective photocatalytic properties of TiO_2 nanotubes in environmental cleanup. In this research, TiO_2 was immobilized onto MMT to serve as a photocatalyst for the removal of Basic Blue 3. Unlike the compounds used in the previously mentioned studies, MMT is a naturally derived clay known for its excellent swelling and adsorption capabilities in aqueous environments.

The MMT/TNTs composite is anticipated to be a highly efficient and environmentally friendly photocatalyst for the removal of organic dyes.

2. Experimental

2.1. Chemicals

Montmorillonite (MMT) was purified from bentonite sourced in Vietnam, following the procedures detailed in our recent publications [13, 14]. Titanium(IV) Oxide (TiO_2) in the anatase phase was acquired from Merck (purity ≥ 99.8%). Sodium hydroxide (NaOH) and nitric acid (HNO_3), with purities of ≥ 96% and ≥ 86% respectively, were sourced from China. Basic Blue 3 dye was obtained from Sigma-Aldrich, with a dye content of 25%.

2.2. Preparation of TiO_2 nanotubes (TNTs)

Titanium dioxide nanotubes (TNTs) were synthesized using a hydrothermal method. First, a 10 M NaOH solution was prepared. TiO_2 powder was then gradually added to the 10 M NaOH solution and stirred magnetically for 4 h. The resulting mixture was transferred to a Teflon-lined stainless steel autoclave (Figure 1) and heated to 130 °C for 24 h. After naturally cooling to room temperature, the solution was washed multiple times with deionized water and 2M HNO_3 solution until the pH reached 7. The washed product was then collected by centrifugation and dried at 60 °C for 24 h. Finally, the solid obtained was calcined at 400 °C for 2 h to produce TNTs. These steps are illustrated in Figure 1.

2.3. Preparation of MMT/TNTs nanocomposite

The preparation of the MMT/TNTs nanocomposite was conducted following the procedure outlined in our previous publication [14]. First, MMT was dispersed in a beaker containing deionized water and stirred for 24 h to ensure complete swelling. Next, a specific number of TNTs was added to the MMT suspension, followed by 4 h of stirring and 1 h of sonication. The resulting product was collected by centrifugation and then dried at 80 °C for 24 h to yield the MMT/TNTs nanocomposite (Figure 2).

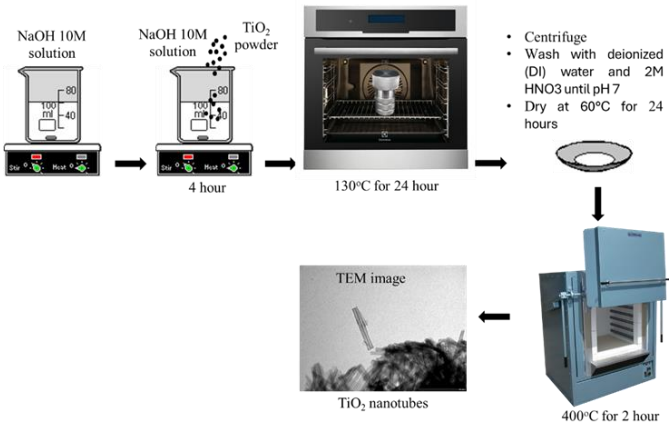

Figure 1 Steps for preparing TNTs.

 DOI: 10.15826/chimtech.2024.11.4.09

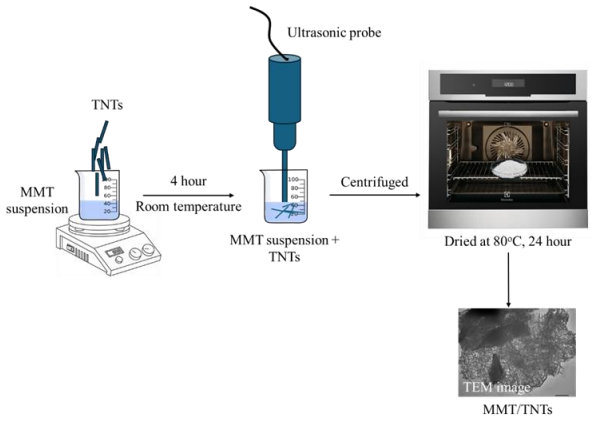

Figure 2 Steps for preparing MMT/TNTs.

2.4. Characteristic methods and experimental setup

The characteristics of the samples were evaluated using the following analytical methods: X-ray diffraction (XRD, D2-PHASER, Germany), transmission electron microscopy (TEM, JEM-1400Plus, USA), Fourier transform infrared spectroscopy (FTIR, Frontier FT-IR/NIR, USA), energy-dispersive X-ray spectroscopy (EDX, HORIBA H-7593, Horiba, Japan), and Brunauer-Emmett-Teller analysis (BET, NOVA 1000e Quantachrome instrument, USA). The experimental setup and efficiency calculations aligned with established photocatalytic literature [15–18]. All adsorption and photocatalytic experiments were performed in a sealed dark chamber to eliminate the influence of ambient light. Adsorption experiments were conducted before activating the UVC lamp, allowing the solution to reach adsorption-desorption equilibrium. The concentration of BB3 before and after the adsorption-photocatalytic experiments was measured using Ultraviolet-visible spectrophotometry (UV-Vis, V730 Jasco, Japan), and by-products were analyzed using Liquid chromatography-mass spectrometry (LC-MS, XEVO Waters, USA).

3. Results and Discussion

As illustrated in Figure 3, the initial TiO_2 powder exhibits a spherical shape with a diameter of less than 100 nm (Figure 3a). Following hydrothermal treatment, TiO_2 transforms into nanotubes (TNTs), with each nanotube measuring approximately 110 nm in length and 5 nm in diameter, oriented in various directions (Figure 3b). Under high temperature and pressure, the Ti–O–Ti bonds in the TiO_2 structure are disrupted. Ti^{4+} (or Ti^{3+}) ions exchange with Na^+ ions in the solution, forming Ti–O–Na bonds. During this process, as the solution is neutralized or acidified, the Na^+ ions are gradually replaced by H^+ ions, forming Ti–OH bonds. The dehydration of these Ti–OH bonds results in the creation of Ti–O–Ti bonds or Ti–O–...–H–O–Ti hydrogen bonds. Ultimately, the Ti–O–Ti bonds may connect at their ends to form the TiO_2 nanotube structure [19, 20]. MMT appears as sheets [21, 22] with a minimum size of 500 nm (Figure 3c). In contrast, the MMT/TNTs nanocomposite reveals that the TNTs are randomly distributed on the surface or interwoven among the MMT sheets (Figure 3d). The elemental composition of MMT/TNTs includes elements commonly found in MMT, such as K, Ca, O, Fe, Na, Mg, Al, and Si [23, 24]. Additionally, a small amount of Ti is present, accounting for 5.2% by weight or 2.23% by atomic percentage (Figure 4).

According to the XRD pattern (Figure 5), the TiO_2 used as the starting material is in the anatase phase, with a characteristic A (101) peak at $2\theta = 25.3°$ (referred to from JCPDS No.21-1272 [25]). However, the diffraction peaks of the TNTs do not correspond to the anatase phase, indicating a structural transformation from particles to nanotubes [26]. This transformation can be attributed to the synthesis process of TNTs from TiO_2, which typically involves the alkalization of TiO_2 at high temperatures in a strong alkaline environment. This process leads to the restructuring of Ti and O atoms, resulting in the formation of titanate nanotube structures with properties distinct from those of the original TiO_2 particles.

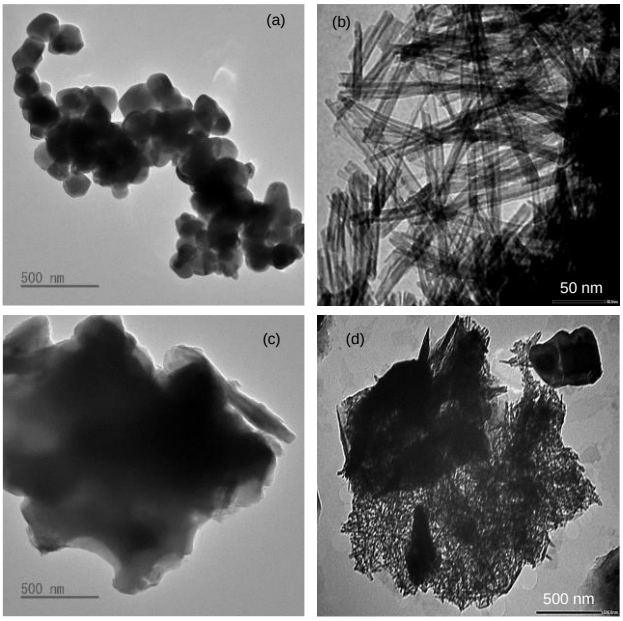

Figure 3 TEM images of TiO_2 powder (a), TNTs (b), MMT (c), and MMT/TNTs (d).

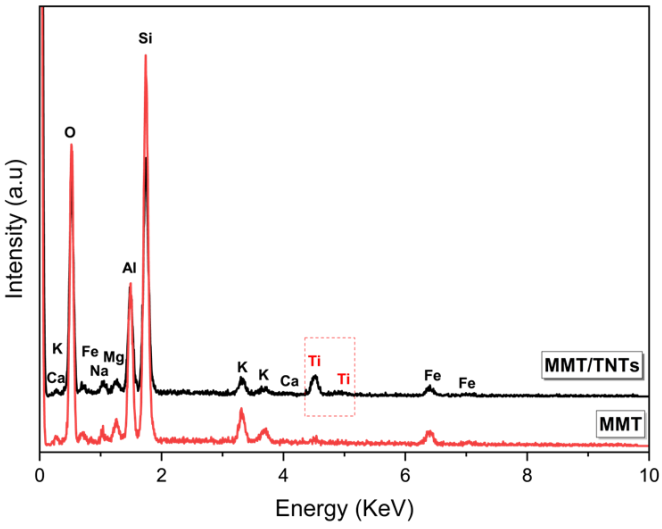

Figure 4 EDX spectra of MMT and MMT/TNTs.

 DOI: 10.15826/chimtech.2024.11.4.09

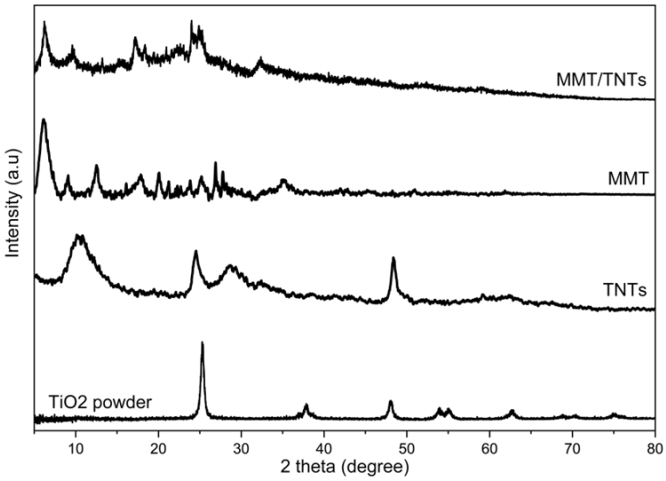

Figure 5 XRD patterns of TNTs, MMT, and MMT/TNTs.

MMT exhibits a preferred orientation at 2θ = 6.1°, corresponding to the (001) plane, with an interlayer spacing of 14.48 Å. Due to the relatively low content of TNTs in the MMT/TNTs composite, the diffraction peaks primarily reflect the characteristic structure of MMT. This suggests that the diffraction properties of MMT remain dominant in the MMT/TNTs composite, although the presence of TNTs may introduce minor alterations in the overall structure.

The crystallinity and crystal sizes of TiO_2, TNTs, MMT, and MMT/TNTs were calculated using equations (1) and (2) [27]. TiO_2 shows a crystallinity of 48.11% with the crystallite size of 3.41 Å, while TNTs exhibit a higher crystallinity of 59.89% with the crystallite size of 0.54 Å, likely due to the structural ordering during nanotube formation. In contrast, MMT has a lower crystallinity of 25.70%, which further decreases to 17.22% in the MMT/TNT composite, possibly due to the introduction of TNTs disrupting the MMT's ordered structure. The crystal sizes of MMT and MMT/TNTs were 1.08 Å and 1.10 Å, respectively.

$$\text{Crystallinity } \% = \left[\frac{\text{Area uder crystalline peaks}}{\text{Area under all peaks}}\right] \cdot 100 \qquad (1)$$

$$D = \frac{k\lambda}{\beta \cos\theta}, \qquad (2)$$

where D is the crystallite size in angstroms (Å), k is the Scherrer constant, whose value is most commonly taken as 0.89, λ is the wavelength of the X-ray beam used (1.5406 Å), β is the Full width at half maximum (FWHM) of the peak and θ is the Bragg angle.

Figure 6 presents the Raman spectra of TiO_2, TNTs, MMT, and MMT/TNTs samples. The TiO_2 powder sample exhibits characteristic Raman bands of the anatase phase at 140 cm^{-1} (Eg), 193 cm^{-1} (Eg), 394 cm^{-1} (B1g), 515 cm^{-1} (A1g/B1g), and 636 cm^{-1} (Eg). Notably, the 140 cm^{-1} (Eg) band is the most intense and is the anatase phase's most easily identifiable signature [28–32].

The Raman spectrum of TiO_2 nanotubes (TNTs) is similar to that of the anatase-phase TiO_2. However, changes in the nanostructure may lead to slight shifts in peak positions or variations in band intensities. Specifically, due to the nanoscale dimensions of the TiO_2 nanotubes, a broadening of the Raman peaks can be observed, a common effect associated with smaller particle sizes. This broadening reflects the strong interactions of crystal lattice vibrations at the nanoscale, which reduce crystal symmetry and result in broadened or blurred Raman bands [33].

MMT (montmorillonite) is characterized by a peak at 100 cm^{-1}, indicative of lattice vibrations between the crystal layers in the layered structure of MMT. This peak arises from the vibrations and relative movements between Si–O and Al–O layers, typical of layered silicates. In MMT's layered structure, the silicate layers interact through van der Waals forces and electrostatic interactions, with the peak at 100 cm^{-1} reflecting these interlayer vibrations [34, 35].

When MMT is combined with TiO_2 nanotubes to form the MMT/TNTs sample, the interaction between the silicate layers of MMT and the TiO_2 nanotubes can influence the lattice vibrations. This interaction may result in shifts in peak positions, changes in intensity, or broadening of the Raman bands, particularly the 100 cm^{-1} peak. Additionally, the combination may induce spectral changes due to size effects and interactions between MMT and TNTs. Such interactions may modify the intensity of the characteristic anatase TiO_2 bands (e.g., the 140 cm^{-1} and 636 cm^{-1} peaks), which can manifest as reduced intensity or broadening due to the dispersion and interaction of TNTs within the layered MMT structure.

Figure 7 presents the N_2 adsorption-desorption isotherms for the TiO_2, TNTs, MMT, and MMT/TNTs samples, with corresponding parameters summarized in Table 1. All samples exhibit a characteristic type IV isotherm with a prominent hysteresis loop, indicative of mesoporous structures.

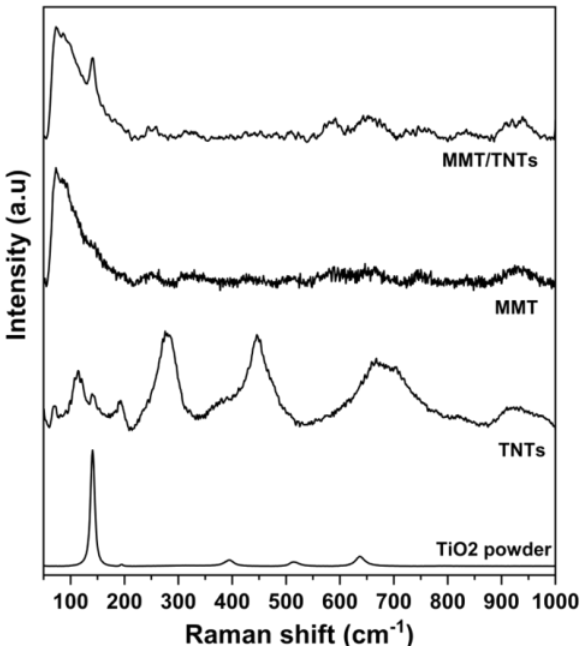

Figure 6 Raman spectra of TNTs, MMT, and MMT/TNTs.

 DOI: 10.15826/chimtech.2024.11.4.09

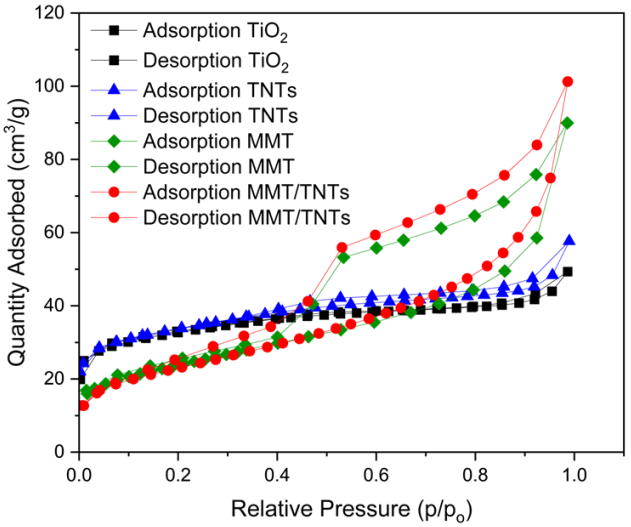

Figure 7 N_2 adsorption-desorption isotherms of TiO_2, TNTs, MMT, and MMT/TNTs.

Table 1 Textural characteristics of TiO_2, TNTs, MMT, and MMT/TNTs.

Samples	BET surface area (m^2/g)	Pore diameter (Å)	Pore volume (cm^3/g)
TiO_2	20.5	5.6	0.080
TNTs	45.2	9.9	0.082
MMT	83.2	40.9	0.134
MMT/TNTs	113.1	32.2	0.162

TiO_2 displays the lowest adsorption capacity, reflecting its limited surface area (20.5 m^2/g) [36, 37]. In contrast, TNTs show a higher adsorption capacity due to their nanotube structure, which provides a larger surface area (45.2 m^2/g) compared to particle structures. This increased surface area offers more active sites for interaction with adsorbate molecules (such as N_2), facilitating more efficient adsorption [37]. MMT exhibits superior adsorption capacity compared to both TiO_2 and TNTs, likely due to its layered structure, which provides additional adsorption sites. Notably, the MMT/TNTs composite achieves the highest adsorption capacity, suggesting that the combination of MMT and TNTs enhances both surface area and adsorption performance. This underscores the potential of MMT/TNTs in applications that require large adsorption surfaces, such as catalysis, filtration, or energy storage.

The optical properties of MMT, TNTs, and MMT/TNTs were analyzed using UV-Vis DRS as a function of the absorption coefficient to wavelength (Figure 8a). All three materials—MMT, TNTs, and MMT/TNTs—exhibited strong absorption in the UV region. The optical bandgap energy from the absorption edges was calculated using Equation 3 [38]. The Tauc plot, based on the direct allowed transition, was validated by plotting $(\alpha h\upsilon)^2$ as a function of photon energy ($h\upsilon$) [39, 40]. The optical bandgap energies of MMT, TNTs, and MMT/TNTs were determined to be 2.75, 3.12, and 3.07 eV, respectively (Figure 8b). These values indicate that while incorporating MMT into the TNT structure slightly reduces the bandgap compared to pure TNTs, it still retains sufficient energy for effective photocatalytic activity in the UV region. This suggests that the MMT/TNTs composite can potentially combine the advantages of both components, enhancing photocatalytic performance through improved adsorption and light absorption properties.

$$(\alpha h\upsilon)^n = C\left(h\upsilon - E_g\right), \quad (3)$$

where $h\upsilon$ is the incident light energy(eV), υ is the photon frequency, α is the adsorption coefficient, C is the energy-dependent constant, m *is* the factor that depends on the nature of the electron transition and is equal to 1/2 or 2 for the indirect or direct transition band gaps, and E_g is the band gap energy (eV).

Figure 9 illustrates the differential efficiency of BB3 dye decolorization under non-irradiated (adsorption) and UVC-irradiated (photocatalytic) conditions. During the adsorption experiment conducted in the dark (Figure 9a), the TNTs sample demonstrated the lowest adsorption capacity, with the C/Co value remaining nearly unchanged and persistently high after 240 minutes (C/Co ≈ 0.9). In contrast, the MMT sample exhibited better adsorption performance, characterized by a substantial reduction in C/Co within a short duration, stabilizing at approximately 0.4. The MMT/TNTs composite outperformed both individual components, with the C/Co ratio gradually declining to around 0.2, indicating that the integration of MMT with TNTs markedly enhanced the material's adsorption capacity.

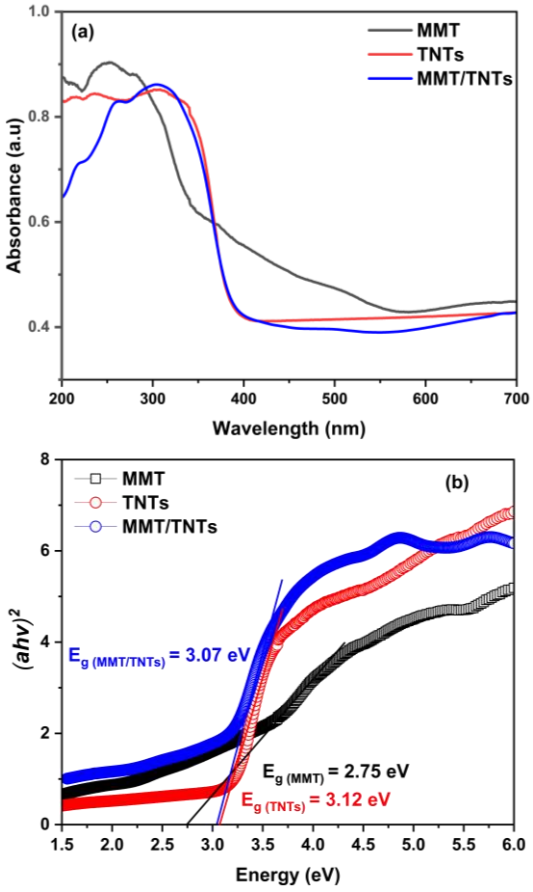

Figure 8 UV-Vis DRS spectrum (a); and Tauc's plot showing optical bandgap energies (b) of MMT, TNTs, and MMT/TNTs.

 DOI: 10.15826/chimtech.2024.11.4.09

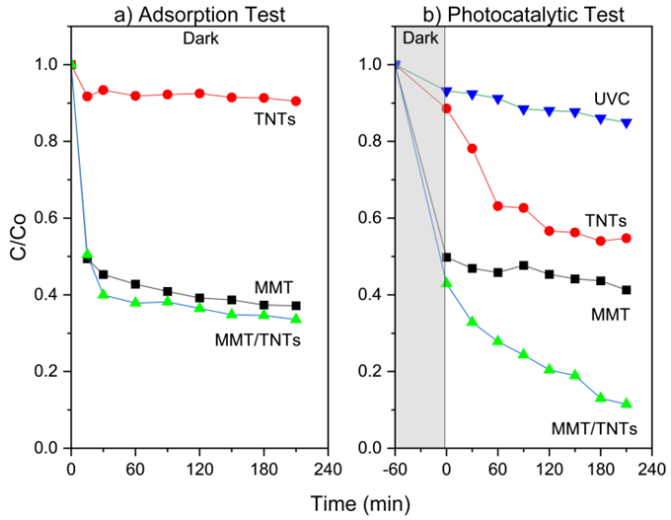

Figure 9 Adsorption – photocatalytic experiments of MMT, TNTs, MMT/TNTs.

This improvement can be attributed to the increased surface area provided by the nanostructured TiO_2 nanotubes within the composite, facilitating more efficient access of pollutant molecules to the active sites. Additionally, the TiO_2 nanotubes may introduce surface charge effects, further contributing to pollutant molecules' effective trapping and retention [41, 42].

In the photocatalytic experiment (Figure 9b), the initial adsorption process under dark conditions yields similar results (time axis from –60 to 0), with the MMT/TNTs sample continuing to demonstrate the best adsorption capacity. When UVC light is introduced, the MMT/TNTs sample exhibits superior performance, showing a significant decrease in C/Co from the onset of illumination and a steady decline over time. In contrast, the TNTs and MMT samples exhibit poorer photocatalytic efficiency, with C/Co decreasing more slowly and remaining at higher levels compared to MMT/TNTs. This indicates that the combination of MMT and TNTs enhances adsorption capacity and improves photocatalytic efficiency. Titanium dioxide (TiO_2), the principal component of TNTs, is a widely used semiconductor in photocatalysis due to its ability to generate electron-hole pairs when exposed to UV light. These electron-hole pairs can react with water and oxygen in the environment to produce free radicals, such as hydroxyl (OH·) and superoxide ($O_2\cdot^-$), which possess strong oxidative properties and can effectively break down organic pollutants [43, 44]. When TNTs are combined with MMT, the dispersion of TNTs is improved thanks to MMT's layered structure, leading to enhanced contact between pollutants and photocatalytic active sites. Moreover, MMT can further enhance the separation of electron-hole pairs by retaining or transferring electrons, thereby reducing recombination processes and improving the system's photocatalytic performance [45, 46]. In summary, the combination of MMT and TNTs creates a composite material that leverages the strengths of both components: MMT's strong adsorption capacity and TNTs' high photocatalytic efficiency. This combination not only improves the ability to handle pollutants but also significantly boosts the effectiveness of organic pollutant degradation under light exposure.

Figure 10 illustrates the effect of catalyst concentration and BB3 concentration on photocatalytic efficiency, as indicated by the C/Co ratio after the reaction. Figure 10a shows that as the catalyst concentration increases from 0.05 g/L to 0.30 g/L, the C/Co ratio decreases sharply from approximately 0.20 to nearly 0.0. This indicates a significant improvement in photocatalytic efficiency with higher catalyst amounts. This can be explained by the fact that as the catalyst concentration rises, the number of active sites on the catalyst surface also increases. This enhances the generation of free radicals (OH·, $O_2\cdot^-$) during the photocatalytic reaction, thereby improving the degradation efficiency of the BB3 pollutant. However, it is important to note that beyond a certain level further increases in catalyst concentration may not lead to significant benefits or might even reduce performance due to light saturation or excessive light scattering in the solution [47, 48].

The impact of the initial concentration of BB3 on photocatalytic efficiency is illustrated in Figure 10b. It shows that as the initial concentration of BB3 increases from 5 ppm to 25 ppm, the C/Co ratio also increases, indicating a reduction in photocatalytic efficiency. The C/Co ratio rises from nearly 0.0 at 5 ppm to around 0.20 at 25 ppm. This can be explained by the fact that as the BB3 concentration increases, the number of BB3 molecules in the solution also rises. This results in competition among BB3 molecules for access to the active sites on the catalyst surface, reducing the likelihood of individual BB3 molecules interacting with the free radicals generated during the photocatalytic process. Additionally, a high concentration of BB3 can diminish light penetration into the solution, thereby reducing the effectiveness of the photocatalytic reaction [49, 50]. Therefore, to achieve optimal photocatalytic efficiency, it is crucial to control both the catalyst amount and the initial pollutant concentration.

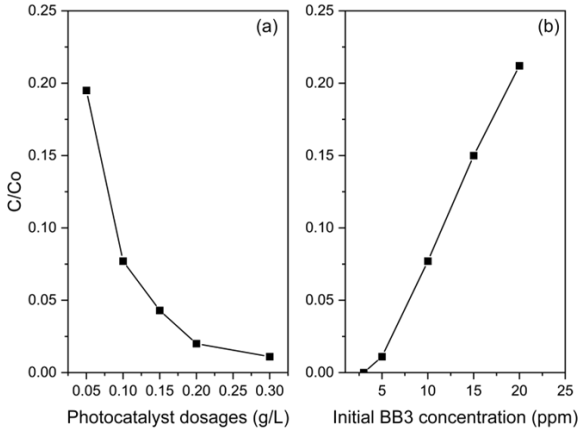

Figure 10 Effect of the MMT/TNTs dosages (a), and the initial RhB concentration (b) on the photocatalytic of RhB under UVC 15 W.

 DOI: 10.15826/chimtech.2024.11.4.09

Table 2 Comparing the removal efficacy of MMT/TNTs for the degradation of basic blue 3 with other studies.

Photocatalyst	Concentration of BB3 (ppm)	Light source	Photocatalyst amount (g/L)	Removal efficacy (%)	Ref.
MMT/TNTs	10	UVC 15 W	0.1	95	This study
TiO_2/MMT	10	Ultrasonic 300 W	1	80	[51]
Response Surface Methodology (RSM)	10	UV/H_2O_2 30 W	–	95.06	[52]
$K_2S_2O_8$	10	UVC 30 W	0.250	80	[53]
TiO_2/Fe_2O_3	3	Direct sunlight irradiation	0.001	92.5	[54]

Compared to the recent studies on the removal of BB3 using various photocatalysts, as summarized in Table 2, MMT/TNTs demonstrate highly competitive performance. Specifically, with a BB3 concentration of 10 ppm, a photocatalyst dosage of 0.1 g/L, and under UVC light, the MMT/TNTs composite achieved a 95% removal efficiency. This is notably higher than the TiO_2/MMT catalyst, which required a significantly larger amount of photocatalyst (1 g/L) and ultrasonic irradiation to reach 80% efficacy.

In comparison with other advanced systems, such as those using the Response Surface Methodology (RSM) and $K_2S_2O_8$, which reached removal efficiencies of 95.06% and 80%, respectively, the MMT/TNTs composite shows similar or superior performance with a much lower catalyst dosage and lower energy consumption, as it requires only a 15 W UVC light source. Additionally, although the TiO_2/Fe_2O_3 catalyst achieved a comparable removal efficiency of 92.5% under direct sunlight, it was tested at a lower concentration of BB3 (3 ppm), making the MMT/TNTs catalyst more efficient under higher pollutant concentrations.

These comparisons highlight the significant potential of MMT/TNTs for efficient dye degradation, particularly in terms of lower energy requirements and minimal catalyst dosage.

4. Limitation

One of the limitations of this study is the unavailability of certain advanced analytical methods, such as PL and SAED, due to the constraints of the local equipment.

5. Conclusions

We successfully synthesized a nanocomposite (MMT/TNTs) by combining montmorillonite (MMT) and TiO_2 nanotubes (TNTs), and demonstrated its potential as an efficient photocatalyst for the degradation of organic dyes in wastewater under UVC irradiation. The nanocomposite exhibited dual functionalities: MMT contributed to dye adsorption, while TNTs provided photocatalytic activity. With a dye degradation efficiency of 95%, significantly outperforming pristine MMT and TNTs, MMT/TNTs offer a promising and sustainable approach to wastewater treatment. This research highlights the feasibility of using naturally sourced materials for advanced environmental remediation applications.

• Supplementary materials

No supplementary materials are available.

• Funding

This research had no external funding.

• Acknowledgments

This research is funded by the University of Science, VNU-HCM under grant number T2023-155. This work was also supported by the Laboratory of Fundamental Materials Science - Faculty of Materials Science and Technology from the University of Science, Viet Nam National University Ho Chi Minh City (VNUHCM-US or HCMUS).

• Author contributions

Conceptualization: B.T.T.D., C.N.H.T.
Data curation: B.T.T.D.
Formal Analysis: B.T.T.D.
Investigation: B.T.T.D., H.N.L., T.D.N.
Methodology: H.N.L.
Project administration: B.T.T.D., C.N.H.T.
Software: B.T.T.D.
Supervision: B.T.T.D., C.N.H.T.
Validation: C.N.H.T.
Visualization: H.N.L., T.D.N.
Writing – original draft: B.T.T.D.
Writing – review & editing: B.T.T.D., C.N.H.T.

• Conflict of interest

The authors declare no conflict of interest.

• Additional information

Author IDs:
Bang Tam Thi Dao, Scopus ID 56400317700;
Trung Do Nguyen, Scopus ID 57223276440;
Hon Nhien Le, Scopus ID 57223279325;
Chi-Nhan Ha-Thuc, Scopus ID 55233663200.

 DOI: 10.15826/chimtech.2024.11.4.09

Websites:

Viet Nam National University Ho Chi Minh City, https://en.hcmus.edu.vn/;

Vietnam National University Ho Chi Minh City, https://vnuhcm.edu.vn/.

References

1. Jianli W, Qingjia S, Biyang T, Cheng G. Photodegradation of dye wastewater by Ti-doped Bi_2O_3/montmorillonite composites. Desalinat Water Treatment. 2024;319:100541. doi:10.1016/j.dwt.2024.100541
2. Licai C, Yunliang Z, Tianxing C, Haoyu , Tingting Z, Hongqiang L, Qing A, Shaoxian S. Correlation of aspect ratio of montmorillonite nanosheets with the colloidal properties in aqueous solutions. Res Phys. 2019;15:102526. doi:10.1016/j.rinp.2019.102526
3. Alastair TMM, Sreejith K, Susan AB. Structural features of thermally or mechano-chemically treated montmorillonite clays as precursors for alkali-activated cements production. Cement Concrete Res. 2024;181:107546. doi:10.1016/j.cemconres.2024.107546
4. Nahid Y, Mahdi M, Reza D. Montmorillonite clay: Introduction and evaluation of its applications in different organic syntheses as catalyst: A review. Res Chem. 2022;4:100549. doi:10.1016/j.rechem.2022.100549
5. Nasim U, Zarshad A, Amir, Sada K, Bushra A, Asma N, Sher BK. Preparation and dye adsorption properties of activated carbon/clay/sodium alginate composite hydrogel membranes. RSC Adv. 2024;14(1,2):211–221. doi:10.1039/d3ra07554k
6. Tarmizi T, Andika M, Nurul M, Syamsuddin MW, Patimah MSBNS, Neza RP, Aldes L, Yudha GW. Synthesis and characterization of montmorillonite – Mixed metal oxide composite and its adsorption performance for anionic and cationic dyes removal. Inorg Chem Commun. 2023;147:110231. doi:10.1016/j.inoche.2022.110231
7. Biyang T, Shengqing W, Haichun X, Jianli W, Yuying M. Optimization of preparation conditions of Bi-doped TiO_2/montmorillonite composites and its photodegradation of Rhodamine B. Desalinat Water Treat. 2024;318:100328. doi:10.1016/j.dwt.2024.100328.
8. Zahra S, Zahra H, Parisa M, Aydin H. Preparation of novel and low-cost chitosan modified with montmorillonite/ZnO hydrogel nanocomposite for adsorption of ciprofloxacin from water. J Water Proc Engin. 2024;63:105449. doi:10.1016/j.jwpe.2024.105449
9. Soumya RM, Ahmaruzzaman M. CuO and CuO-based nanocomposites: Synthesis and applications in environment and energy. Sustainable Mater Technol. 2022;33:E00463. doi:10.1016/j.susmat.2022.e00463
10. Elika SG, Zahra GJ, Amir A, Marzieh G, Azin K, Anita PK, Mitra M, Monireh AH, Jahan BG, Xuanhua L. TiO_2 nanotube/$ZnIn_2S_4$ nanoflower composite with step-scheme heterojunction for efficient photocatalytic H_2O_2 production and organic dye degradation. J Environm Chem Engin. 2023;11(3):110160. doi:10.1016/j.jece.2023.110160
11. Qinyao W, Yuhua Z, Zieng Z, Shengwen L, Yadan D, Xiang W, Qilu Y, Kesheng W. Hydrothermal preparation of Sn_3O_4/TiO_2 nanotube arrays as effective photocatalysts for boosting photocatalytic dye degradation and hydrogen production. Ceram Int. 2023;49(4):5977–5985. doi:10.1016/j.ceramint.2022.11.113
12. Yu-Long X, Li-Fang G, Cuo-Ji B. Fabrication of BiOI Nanoflowers Decorated TiO_2 Nanotube Arrays on Porous Titanium with Enhanced Photocatalytic Performance for Rhodamine B Degradation. Int J Electrochem Sci. 2022;17(2):22022. doi:10.20964/2022.02.04.
13. Tam TBD, Loan TTH, Do TN, Nhien HL, Quoc KL, Truong HN, Chi-Nhan HT. Vietnamese Montmorillonite Supported ZnO: Preparation, Characterization, and Photocatalytic Enhancement in Degradation of Rhodamine B. Kinetics Catalysis. 2023;64(4):390–402. doi:10.1134/S002315842304002X
14. Tam TBD, Loan TTH, Nhien HL, Do TN, Truong HN, Chi-Nhan HT. Characterization and the Effect of Different Parameters on Photocatalytic Activity of Montmorillonite/TiO_2 Nanocomposite under UVC Irradiation. Periodica Polytechnica Chem Engin. 2024;68(1):35–49. doi:10.3311/PPch.22065
15. Mehrnaz G, Narges EF, Mehdi G, Mohammad TY. Bimetal Cu/Ni-BTC@SiO_2 metal-organic framework as high-performance photocatalyst for degradation of azo dyes under visible light irradiation. Environm Res. 2024;256:119229. doi:10.1016/j.envres.2024.119229
16. Elham AA, Poonam D, Bushra F, Sumbul H, Sharf IS, Seungdae O. Cu-Zn coupled heterojunction photocatalyst for dye degradation: Performance evaluation based on the quantum yield and figure of merit. J Saudi Chem Soc. 2024;28(3):101858. doi:10.1016/j.jscs.2024.101858
17. Adhitiyan T, Dhanaraj K, Gubendhiran S, Suresh G, Thenpandiyan E, Prasath M. Green Synthesized Silver And Zinc Doped Hydroxyapatite Photocatalysts To Remove Methylene Blue And Rhodamine B Dyes From Industrial Wastewater. Chem Phys Impact. 2024;100695. doi:10.1016/j.chphi.2024.100695
18. Bayahia H. Schinus molle extract mediated green synthesis of iron niobate photocatalyst for the degradation of methyl orange dye under visible light. J Saudi Chem Soc. 2024;28(3):101876. doi:10.1016/j.jscs.2024.101876
19. Chen H, Chen D, Bai L, Shu K. Hydrothermal Synthesis and Electrochemical Properties of TiO_2 Nanotubes as an Anode Material for Lithium Ion Batteries. Int J Electrochem Sci. 2018;13:2118–2125. doi:10.20964/2018.02.75
20. Zavala MAL, Morales SAL, Ávila-Santos M. Synthesis of stable TiO_2 nanotubes: effect of hydrothermal treatment, acid washing and annealing temperature. Heliyon. 2017;3(11):e00456. doi:10.1016/j.heliyon.2017.e00456
21. Venkatesha NJ, Prakash BSJ, Bhat YS. The active site accessibility aspect of montmorillonite for ketone yield inester rearrangement. Catal Sci Technol. 2015;5:1629. doi:10.1039/C4CY01356E
22. Cai W, Zhu X, Kumar R, Zhu Z, Ye J, Zhao J. Catalytic Pyrolysis of Biomass Waste using Montmorillonite-Supported Ultrafine Iron Nanoparticles for Enhanced Bio-Oil Yield and Quality. Green Energy Resources. 2024;100085. doi:10.1016/j.gerr.2024.100085
23. Wang J, Su Q, Tuo B, Gan C. Photodegradation of dye wastewater by Ti-doped Bi_2O_3/montmorillonite composites. Desalination Water Treat. 2024;319:100541. doi:10.1016/j.dwt.2024.100541
24. Makwana D, Castan J, Somani RS, Bajaj HC. Characterization of Agar-CMC/Ag-MMT nanocomposite and evaluation of antibacterial and mechanical properties for packaging applications. Arab J Chem. 2020;13(1):3092-3099. doi:10.1016/j.arabjc.2018.08.017
25. Shuang S, Ruitao L, Zheng X, Zhengjun Z. Surface Plasmon Enhanced Photocatalysis of Au/Pt-decorated TiO_2 Nanopillar Arrays. Sci Rep. 2016;6:26670. doi:10.1038/srep26670
26. Rendón-Rivera A, Toledo-Antonio JA, Cortés-Jácome MA, Angeles-Chávez C. Generation of highly reactive OH groups at the surface of TiO_2 nanotubes. Catalysis Today. 2011;166:18–24. doi:10.1016/j.cattod.2010.03.045
27. Soumya RM, Vishal G, Kshitij RBS, Shyam SP, Ahmaruzzaman M.Developing In_2S_3 upon modified $MgTiO_3$ anchored on nitrogen-doped CNT for sustainable sensing and removal of toxic insecticide clothianidin. Environ Res. 2024;259:119435. doi:10.1016/j.envres.2024.119435
28. Wu Z, Zhao H, Zhou X, Wang Y, Zuo K, Cheng H. Thermal Migration Behavior of Na^+, Cu^{2+} and Li^+ in Montmorillonite. Minerals. 2022;12(4):477. doi:10.3390/min12040477
29. Nanjegowda VH, Biligiri KP, Asce KP, Mahimaluru J, Mondal D. Development of Organoclay Suitable for Applications in Recycled Rubber–Based Asphalt Binders: Montmorillonite Tailored with QuaternaryAmmonium Salt. J Mater Civ Eng.

 DOI: 10.15826/chimtech.2024.11.4.09

2023;35(1):04022390. doi:10.1061/(ASCE)MT.1943-5533.0004578
30. El-Deen SS, Hashem AM, Ghany AEA, Indris S, Ehrenberg H, Mauger H, Julien CM. Anatase TiO_2 nanoparticles for lithium-ion batteries. Ionics. 2018;24:2925–2934. doi:10.1007/s11581-017-2425-y
31. Challagulla S, Tarafder K, Ganesan R, Roy S. Structure sensitive photocatalytic reduction of nitroarenes over TiO_2. Sci Rep. 2017;7:8783. doi:10.1038/s41598-017-08599-2
32. Scrimieri L, Velardi L, Serra A, Manno D, Ferrari F, Cantarella M, Calcagnile L. Enhanced adsorption capacity of porous titanium dioxide nanoparticles synthesized in alkaline sol. Appl Phys A. 2020;126:926. doi:10.1007/s00339-020-04103-2
33. Soto PC, Salamanca-Neto CAR, Moraes JT, Sartori ER, Bessegato GG, Lopes F, Almeida LC. A novel sensing platform based on self-doped TiO_2 nanotubes for methylene blue dye electrochemical monitoring during its electro-Fenton degradation. J Solid State Electrochem. 2020;24:1951–1959. doi:10.1007/s10008-020-04509-1
34. Muñoz-Iglesias V, Sánchez-García L, Carrizo D, Molina A, Fernández-Sampedro M, Prieto-Ballesteros O. Raman spectroscopic peculiarities of Icelandic poorly crystalline minerals and their implications for Mars exploration. Sci Rep. 2022;12:5640. doi:10.1038/s41598-022-09684-x
35. Wang A, Freeman JJ, Jolliff BL. Understanding the Raman spectral features of phyllosilicates. J Raman Spectrosc. 2015;93555151. doi:10.1002/jrs.4680
36. Shaikh SF, Mane RS, Min BK, Hwang YJ, Oh-shim J. D-sorbitol-induced phase control of TiO_2 nanoparticles and its application for dye-sensitized solar cells. Sci Rep. 2015;6(1):20103. doi:10.1038/srep20103
37. Ong WL, Ho GW. Enhanced Photocatalytic Performance of TiO_2 Hierarchical Spheres Decorated with Ag_2S Nanoparticles. Procedia Engin. 2016;141:7–14. doi:10.1016/j.proeng.2015.09.217
38. Saptarshi R, Soumya RMi, Vishal G, Ankur KG, Ahmaruzzaman M. Anchoring Ni(II) bisacetylacetonate complex into CuS immobilized MOF for enhanced removal of tinidazole and metronidazole. Clean Water. 2024;7:83. doi:10.1038/s41545-024-00375-w
39. Kite SV, Sathe DJ, Kadam AN, Chavan SS, Garadkar SS. Highly efficient photodegradation of 4-nitrophenol over the nano-TiO_2 obtained from chemical bath deposition technique. Res Chem Intermediates. 2020;46(2):1255–1282. doi:10.1007/s11164-019-04032-7
40. Miguel ALZ, Samuel ALM, Manuel AS. Synthesis of stable TiO2 nanotubes: effect of hydrothermal treatment, acid washing, and annealing temperature. Heliyon. 2017;3:e00456 . doi:10.1016/j.heliyon.2017.e00456
41. Arifin SNH, Mohamed RMSR, Al-Gheethi AA, Wei LC, Yashni G, Fitriani N, Naushad M, Albadarin AB. Modified TiO_2 nanotubes-zeolite composite photocatalyst: Characteristics, microstructure, and applicability for degrading triclocarban. Chemosphere. 2022;287(3):132278. doi:10.1016/j.chemosphere.2021.132278
42. Paramasivam, Avhale A, Inayat A, Bösmann A, Schmuki P, Schwieger W. MFI-type (ZSM-5) zeolite-filled TiO_2 nanotubes for enhanced photocatalytic activity. Nanotechnol. 2009;2(22):225607. doi:10.1088/0957-4484/20/22/225607
43. Saptarshi R, Soumya RM, Ahmaruzzaman M. Ultrasmall copper-metal organic framework (Cu-MOF) quantum dots decorated on waste derived biochar for enhanced removal of emerging contaminants: Synergistic effect and mechanistic insight. J Environ Manag. 2024;366:121802. doi:10.1016/J.JENVMAN.2024.121802
44. Soumya RM, Vishal G, Ahmaruzzaman M. A critical review on In_2S_3-based nanomaterial for emerging contaminants elimination through integrated adsorption-degradation technique: Effect of reaction parameters and co-existing species. J Hazardous Mater Lett. 2023;4:100087. doi:10.1016/J.HAZL.2023.100087
45. Zhang J, Tan H, Deng X, Li M, Jian S, Li G. Preparation of organic montmorillonite supported TiO_2 and its application in methylene blue removal. Construction Building Mater. 2022;341:127762. doi:10.1016/j.conbuildmat.2022.127762
46. Karunadasa KSP, Wijekoon ASK, Manoratne CH. TiO_2-kaolinite composite photocatalyst for industrial organic waste decontamination. Next Mater. 2024;3:100065. doi:10.1016/j.nxmate.2023.100065
47. Zhao S, Xiao H, Chen Y, Qi Y, Yan C, Ma R, Zhao Q, Liu We, Shen Y. Photocatalytic degradation of xanthates under visible light using heterogeneous CuO/TiO_2/montmorillonite composites. Green Smart Mining Engin. 2024;1(1):67–75. doi:10.1016/j.gsme.2024.03.003
48. Özyürek IN, Kıranşan M, Karaca S. Investigation of the removal of sulfamethoxazole drug waste from aqueous solutions under the effect of zinc oxide/montmorillonite nanocomposite by photocatalytic ozonation process. Desalination Water Treatment. 2021;242:144–161. doi:10.5004/dwt.2021.27847
49. Alahmad W, Hedhili F, Al-Shomar SM, Albaqawi HS, Al-Shammari NA, Abdelrahman S. Modeling Sustainable Photocatalytic Degradation of Acidic Dyes using Jordanian Nano-Kaolin–TiO_2 and Solar Energy: Synergetic Mechanistic Insights. Heliyon. 2024;e36978. doi:10.1016/j.heliyon.2024.e36978
50. El-Dossoki FI, Atwee TM, Hamada AM, El-Bindary AA. Photocatalytic degradation of Remazol Red B and Rhodamine B dyes using TiO_2 nanomaterial: estimation of the effective operating parameters. Desalination Water Treatment. 2021;233:319–330. doi:10.5004/dwt.2021.27519
51. Alireza K, Mohsen S, Aydin H, Mojtaba T, Semra K. Sonocatalytic removal of an organic dye using TiO_2/Montmorillonite nanocomposite. Ultrasonics Sonochem. 2025;22:404–411. doi:10.1016/j.ultsonch.2014.07.002
52. Kasiri MB, Khataee AR. Photooxidative decolorization of two organic dyes with different chemical structures by UV/H_2O_2 process: Experimental design. Desalination. 2011;270(1–3):151–159. doi:10.1016/j.desal.2010.11.039
53. Khataee AR, Mirzajani O. UV/peroxydisulfate oxidation of C. I. Basic Blue 3: Modeling of key factors by artificial neural network. Desalinat. 2010;251:64–69. doi:10.1016/j.desal.2009.09.142
54. Zeinab AS, Achisa CM, Josphat IM. Effect of TiO_2/Fe_2O_3 nanopowder synthesis method on visible light photocatalytic degradation of reactive blue dye. Heliyon. 2024;10(8):e29648. doi: 10.1016/j.heliyon.2024.e29648

 DOI: 10.15826/chimtech.2024.11.4.09